Discriminating the physical impacts of various laser pulses on the magnetic structure of oriented electrical steels

O. Maloberti, M. Nesser, J. Dupuy, P. Dassonvalle, J. Fortin, C. Pineau, J.P. Birat

Discriminating the physical impacts of various laser pulses on the magnetic structure of oriented electrical steels

O. Maloberti[a,b,1], M. Nesser[b], J. Dupuy[c], P. Dassonvalle[a,d], J. Fortin[a,b], C. Pineau[e], J.P. Birat[f]

[a]*SYMADE-UNILASALLE Amiens, 14 quai de la Somme, Amiens, 80080, France ;* [b]*Laboratoire LTI, IUT d'Amiens Avenue des Facultés – Le Bailly, Amiens, 80025, France ;* [c]*Multitel a.s.b.l., 2 Rue Pierre et Marie Curie Parc Initialis, Mons, 7000, Belgique ;* [d]*Laboratoire MIS, UPJV, 14 quai de la Somme, Amiens, 80080, France ;* [e]*IRT-M2P, 4 rue Augustin Fresnel, Metz, 57070, France ;* [f]*IF Steelman, 5 rue du Gate-Chaux, 57280, Semecourt, France*

Pulsed laser technologies with Long (LPL **I**rradiation), Short (SPL **S**cribing) and Ultra-Short (USPL **A**blation) pulse duration can be used on SiFe **G**rain **O**riented **E**lectrical **S**teels (GOES) to refine the domains and reduce the power loss. The corresponding physics related to the magnetic structure is still a subject of research. This paper identifies separate characteristics responsible for the domains structure and the magnetization properties in a GOES sheet processed with the three laser pulses. Magnetic domains based properties are identified thanks to an average dynamic ***μ-ν$_c$-Λ* model**, the **T**ensor **M**agnetic **P**hase **T**heory (**TMPT**), magnetic measurements/observations with the **S**ingle **S**heet **T**ester (**SST**) and the **M**agneto-**O**ptical **I**ndicator **F**ilm (**MOIF**) technique.

Keywords: electrical steels, GOES, pulsed laser, irradiation, scribing, ablation, magnetic structure, magnetization dynamics.

1. Introduction, Context and State of the Art

First studies on 180° domain refinement were carried out using a mechanical scratching method [1] to reduce energy losses in GOES. Then different techniques have been proposed: plasma irradiation [2], spark ablation [3] … Surface laser treatment, first with Long Pulsed Lasers (LPL ≥ 10 ns) or continuous Wave Lasers (CWL), appeared as an elegant non-contact method [4, 6]. Finally, different kinds of lasers in various pulse regimes were used more or less successfully [5, 6]. Recent research investigated advanced Short Pulsed (SPL < 10 ns) and Ultra-Short Pulsed Lasers (USPL < 10 ps) rather than LPL. It led to first comparisons of different pulse durations and its impacts on magnetic behaviors (permeability and losses) [7, 8], while defining a new terminology (see Fig. 1). Observations shew that the LPL process, called Irradiation, induces thermal stresses σ_T in a Heat Affected Zone (HAZ$\propto\delta' p'$) through the coating without removing it. The latter modifies the magnetoelastic energy state of magnetic domains. Thus, for energy minimization reason, misoriented closure domains are locally generated and the 180° domains are refined. The SPL process, called Scribing, generates small grooves by melting and removal of the coating and superficial metal particles. In parallel, the process duration leads to a HAZ and thermal stresses σ_M. In this case, the domains refinement can be induced either by magnetic poles or closure domains at the laser spots. The USPL process, called Ablation, generates deep grooves (or Material Removal Zone, MRZ) by vaporization and removal of the coating and metal particles by minimizing the HAZ. Physical interpretations and correlations between the process parameters and impacts and some magnetic properties have been partially studied [9, 10]. Reference [9] focused on the impacts of LPL and SPL on static and dynamic properties. Reference [10] identified the LPL, SPL and USPL impacts on the Bertotti separated loss coefficients [11]. Distinct physical justifications can be completed with the help of investigation model(s) based on the microscopic domains structure [12, 13]. Distinct physical justifications for the magnetic improvements shall be found with the help of a behavioral and loss model, based on a description of the microscopic magnetic structure with domains and walls. First, the average dynamic μ-ν_c-Λ model [12] will be used to identify the impact of pulsed laser processes on the separated properties μ, ν_c and Λ related to the static internal permeability, coercive field strength and dynamic losses respectively. There, magnetization reversal mechanisms are described with an averaged domains and walls property Λ, lumping the walls' surface S, density n and mobility η. Thus, there is no distinction between the magnetic structure at the sheet surface and the one within the thickness. Hence, the Tensor Magnetic Phase Theory (TMPT) will be used to statistically describe the domains' structure and phases in the mass of the material [13]. Four original material characteristics have to be identified: a stress dependent and anisotropic exchange characteristic κ, a coercive reluctivity ν_c related to the grain boundaries and defects, the surface magnetic structure topological and dynamical properties lumped in a tensor variable $[\Lambda_0^2]$ and finally a dynamic damping characteristic τ, due to the damping magnetization reversal mechanisms, and certainly dependent on the walls mobility. Finally, microscopic observation of the magnetic structure thanks to the MOIF technique will inform about the shape and average size $\langle w \rangle$ of domains at the surface, which makes it possible to value the impact of a pulsed laser separately on both the refinement effect and the walls mobility effect depending on the pulse duration.

2. Description of the experiments

2.1. Laser treatments – process parameters

Three pulsed laser processes performed with a fixed spot size and scanning speed will be looked at (Fig. 1):

- The Long Pulsed Laser process (LPL)* induces thermal stresses σ_T in the Heat Affected Zone (HAZ$\propto\delta' p'$) through the coating without removing it. This configuration will also be called Irradiation.

[1] Corresponding author: olivie.maloberti@gmail.com

- The Short Pulsed Laser process (SPL)* generates a groove by melting and removal of the coating and superficial metal particles. In parallel, the process duration leads to a HAZ and thermal stresses σ_M. This configuration will be called Scribing.
- The Ultra Short Pulsed Laser process (USPL)** generates a deep groove (or Material Removal Zone, MRZ) by vaporization and removal of the coating and metal particles by minimizing the HAZ but generating a plasma and a Laser Induced Shock Wave. This configuration will be called Ablation.

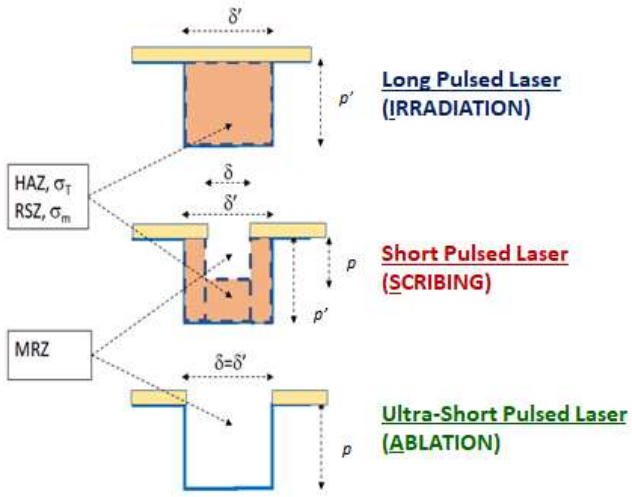

Fig. 1 : The three Pulsed Laser Processes selected.

*LPL and SPL were performed with an IPG pulsed Ytterbium fiber laser with a wavelength of 1.064 µm. It delivers pulse duration between 4 and 200 ns. **USPL was performed with an Ytterbium Amplitude Laser at a wavelength of 1.03 µm with an adjustable pulse width between a few hundreds of fs and 10 ps.

References [7-10] provide optimal parameters to maximize the loss reduction factor up to 20% @ 1.7T 50Hz and minimize the J800 reduction by a factor of 5%. Each configuration corresponds to the optimal amount of energy without: damaging the coating for LPL, inducing critical droplets for SPL and avoiding any recast and sheet deformation for USPL. Table 1 gives relative comparisons between pulse durations Δt *(µs)*, repetition frequencies f_r *(kHz)*, pulse energy densities e_{pulse} *(J.cm^{-2})*, cumulative energy densities e_{cum} *(J.cm^{-2})* and pulse peak power densities p_{peak} *(MW.cm^{-2})* of the 3 selected laser processes (the reference values being the LPL ones).

Table 1 : Main laser configurations

	Δt	f_r	e_{pulse}	e_{cum}	p_{peak}
LPL (I)	**1**	**1**	**1**	**1**	**1**
SPL (S)	**0.04**	**2.5**	**0.4**	**1**	**10**
USPL (A)	**0.000005**	**0.25**	**4.08**	**1.43**	**816327**

2.2. *Specimens: grades and dimensions*

Two conventional grades of $Si_{0.03}Fe_{0.97}$ GOES with thicknesses 0.23 and 0.27 mm will be investigated: grades 23MXX® (specific losses < 1 W/kg @1.7T&50Hz, J800 > 1.7 T) and RXXX27® (specific losses < 1.2 W/kg @1.7T&50Hz, J800 > 1.8 T). Specimens used are squares with size 150*150 mm^2, laser treated either on one or two sides. 7 samples per grade are considered to analyse single pass laser configurations applied on one side (I11, S11, A11) or two sides (I12, S12, A12) in addition to the two passes laser ablation process (USPL 2) on the single-sided sample A21 (Table 2).

Table 2 : List of specimens

SAMPLE	THICKNESS	LASER PROCESS
23I11, 23I12	**0.23 mm**	**LPL IRRADIATION, 1/2 sides**
27I11, 27I12	**0.27 mm**	**LPL IRRADIATION, 1/2 sides**
23S11, 23S12	**0.23 mm**	**SPL SCRIBING, 1/2 sides**
27S11, 27S12	**0.27 mm**	**SPL SCRIBING, 1/2 sides**
23A11, 23A12	**0.23 mm**	**USPL ABLATION 1, 1/2 sides**
27A11, 27A12	**0.27 mm**	**USPL ABLATION 1, 1/2 sides**
23A21	**0.23 mm**	**USPL ABLATION 2, 1 side**
27A21	**0.27 mm**	**USPL ABLATION 2, 1 side**

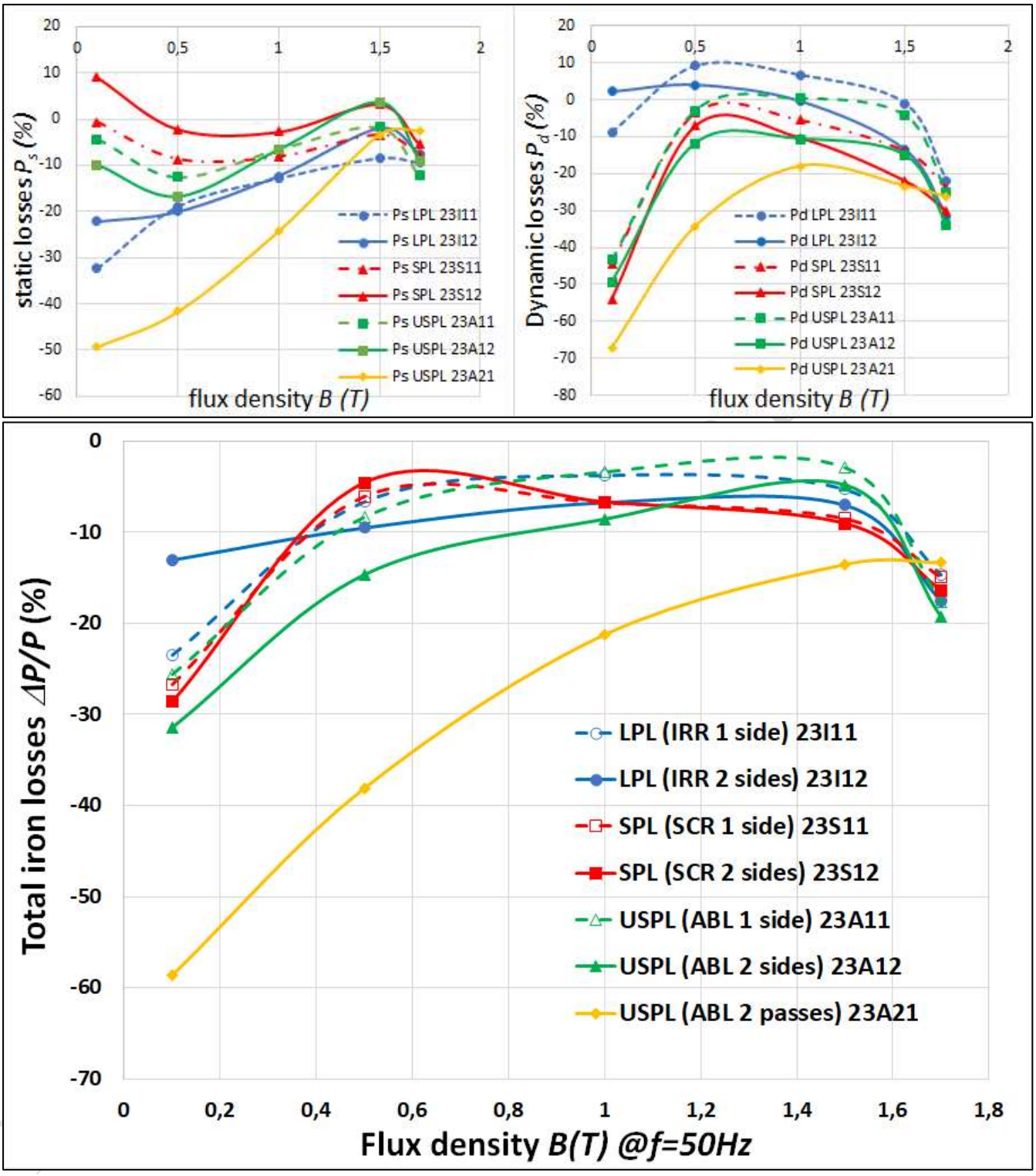

Fig. 2 : Loss reduction properties for LPL (I), SPL (S) and USPL (A) processes on grade 23MXX.

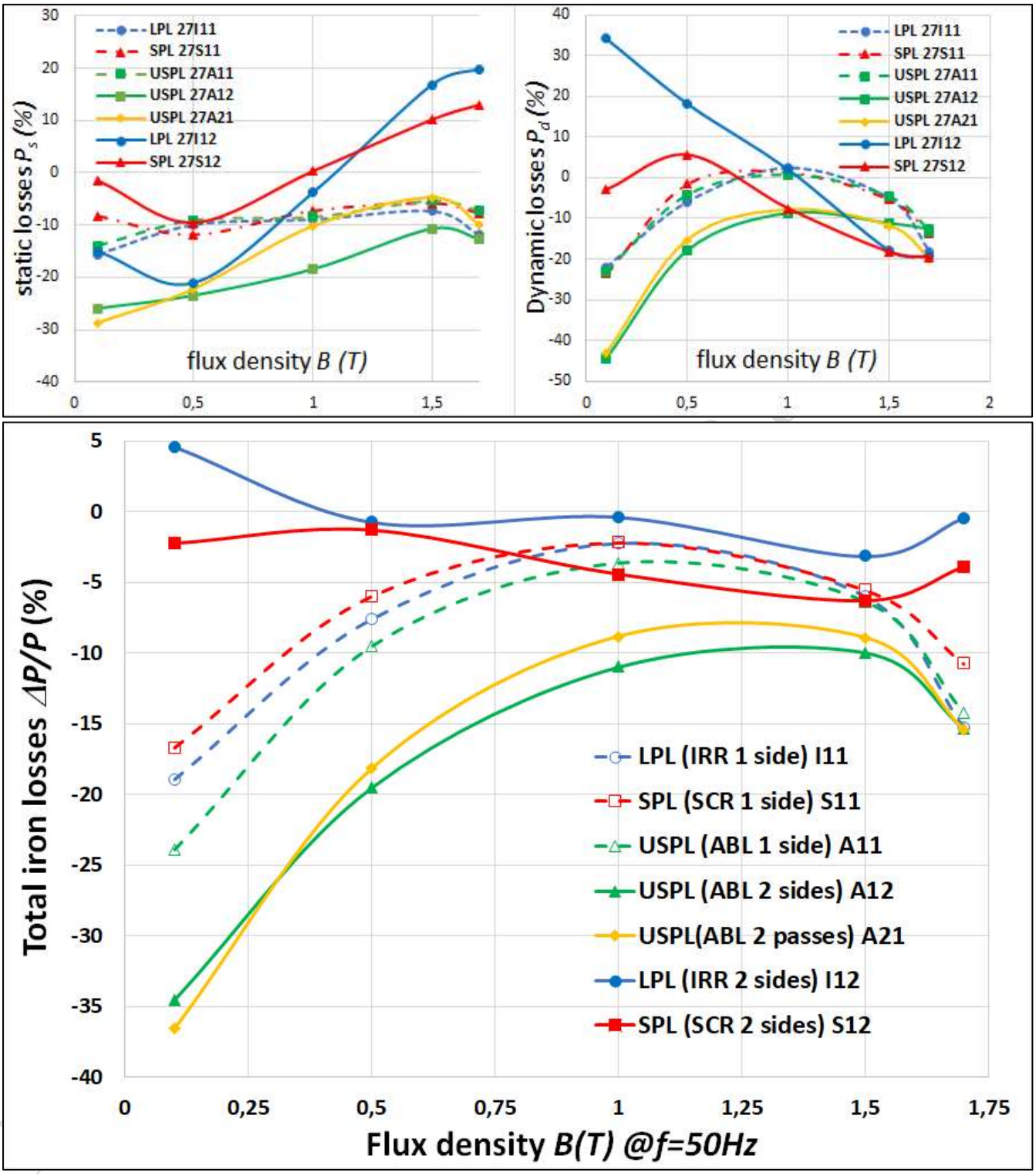

Fig. 3 : Loss reduction properties for LPL (I), SPL (S) and USPL (A) processes on grade RXXX27.

2.1. Magnetic measurements – Single Sheet Tester

The magnetic behaviour and losses of the whole specimens are measured thanks to a Single Sheet Tester (SST 150), providing an accuracy better than 0.5% at high induction and 3% at low induction. Laser treated sheets with thickness 0.23 mm are compared to an average of 16 standard sheets. Laser treated sheets with thickness 0.27 mm are compared before and after the process on same samples.

Fig. 2 and Fig. 3 give the results for both grades 23MXX and RXXX27 respectively as a function of the flux density B. Quasi-static hysteresis losses P_s *(W/kg)* are measured at very low frequency 3-5 Hz (skin depth is more than 3 to 5 times the sheet thickness) and the dynamic losses P_d *(W/kg)* correspond to the whole classical and excess losses that lead to the total losses at usual frequency $f = 50$ Hz. For both grades, the three different pulsed laser processes provide more or less the same loss reduction factor at high induction (1.5 – 1.7 T), the USPL process is the one that shows the highest improvements at low and intermediate induction levels B (0 – 1.5 T), especially with two passes or two sides treatment. In case of single pass and single sided processes, the LPL process is the one that improves the static losses the best. On the contrary, the SPL and USPL are the best options for dynamic losses whatever the number of sides and passes. For the grade RXXX27 with higher thickness, double sided LPL and SPL processes didn't allow any improvement in front of the single sided process, probably due to too much thermal effect required to see any significant impact on such a thickness (up to +6% damage for LPL and +8% damage for SPL). In the next section, we address the questions: which characteristic is the most sensitive to a pulsed laser treatment and what are the origins of the specificity of each pulse duration ? Magnetic measurements will be used to identify the separated properties of two domains based models.

3. Loss models and magnetic properties

3.1. The μ-$\underline{\nu_c}$-Λ model

In this average dynamic μ-$\underline{\nu_c}$-Λ model [12], the total magnetic field H inside the material is separated in three contributions: the static non-dissipative an-hysteretic magnetic field $\mu^{-1}B$ at equilibrium, the quasi-static coercive field strength $j\underline{\nu_c}B$ mainly due to jumps of walls at defects and grains boundaries and the dynamic damping magnetic field $j\omega\sigma\Lambda^2 B$ due to magnetization reversal mechanisms damped by microscopic eddy currents ($\omega = 2\pi f$ is the angle velocity and σ the electrical conductivity). The property $\underline{\nu_c}$ is the coercive reluctivity responsible for the quasi-static losses ($\pi\,\nu_c = K_h$, with K_h the Bertotti coefficient) and is identified with $P_s = \underline{\nu_c}\frac{B^2\omega}{2\pi\gamma}$ (γ is the mass density). μ is defined as the static internal permeability related to the magnetization curve slope. Λ *(μm)* lumps the walls' surface S, density n and mobility η averaged within the thickness. The field diffusion-like equation is then derived from the dynamic field behavior $H = \mu^{-1}B + j\omega\sigma\Lambda^2 B$, the Ohm law and the Maxwell formulae. The field solution of the μ-$\underline{\nu_c}$-Λ model, detailed in [11], provides the apparent permeability μ_{app} (1a) and the dynamic losses P_d (1b) effectively measured, which can be used to identify the impact of pulsed laser processes on the separated properties μ and Λ respectively.

$$\mu_{app} = \frac{B}{H_0} = \frac{\mu_{mag}}{\cos(-\varphi_{mag})} \text{ with } \mu_{mag}e^{j\varphi_{mag}} = \frac{2\mu\tanh((k_+ + ik_-)\zeta/2)}{\zeta(1+i\sigma\Lambda^2\mu\omega)(k_+ + ik_-)} \tag{1a}$$

$$P_d = \frac{\zeta B^2\omega}{4\mu\gamma}\left(\frac{cosh(\zeta k_+)+cos(\zeta k_-)}{sinh^2(\zeta k_+)+sin^2(\zeta k_-)}\right)\begin{pmatrix}(\sigma\Lambda^2\mu\omega k_+ + k_-)\,sinh(\zeta k_+) + \\ (\sigma\Lambda^2\mu\omega — k_+)\,sin(\zeta k_-)\end{pmatrix} \tag{1b}$$

H_0 is the magnetic field applied at the surface, ζ the sheet thickness, $k_\pm$ are the diffusion wave vectors given by (1c) [12]:

$$k_\pm = \sqrt{\frac{1}{2}\left(\frac{\sigma\mu\omega}{1+(\sigma\Lambda^2\mu\omega)^2}\right)}\sqrt{\pm\sigma\Lambda^2\mu\omega + \sqrt{1+(\sigma\Lambda^2\mu\omega)^2}} \tag{1c}$$

3.2. The "Tensor Magnetic Phase Theory" (TMPT)

The investigated TMPT model [13] is put to the test to statistically describe the natural magnetic structuring in the mass of the material with phases and space variations. The domains' structure is represented by a new tensor state variable $[\Lambda^2]$, which stem from a competition between several energy terms at the mesoscopic scale: the magnetic exchange, the magnetic anisotropy, the self-magnetostriction or/and stress induced anisotropy, the dipolar demagnetizing energy (dependent on the boundary condition $[\Lambda_0^2]$) and the dissipated microscopic eddy currents loss (driven by a time delay τ). In case of GOES, $[\Lambda^2]$ is assumed to be diagonal; and a focus on the unknown $\Lambda = \Lambda_{RD}$, representative of the 180° domains in the Rolling Direction (RD), is relevant even if its space distribution is impacted by (closure) domains in other directions. Still using the same surface field behavior as previously, the total energy balance involves four material characteristics: the surface properties lumped in Λ_0, a coercive reluctivity ν_c still related to the grain boundaries and defects, a stress dependent and anisotropic exchange characteristic κ *(mm^{-2})* (ratio between anisotropy plus magneto-striction and magnetic exchange properties) and finally the dynamic damping characteristic τ *(μs)*, certainly dependent on the walls mobility. The TMPT adds a coupling between the surface Λ_0 and the volume property Λ. . Any domains refinement will act on Λ_0, laser induced stress on κ, induced pinning centers on ν_c and any walls nucleation, multiplication and mobility effect will be visible on τ. The 1D solution [12] for $V=\Lambda^{-1}$ (2a), finally provides the mean magnetic polarization J (2b) apparent permeability μ_{app} (2c) the quasi static hysteresis losses P_s (2d) and the dynamic ones P_d (2e):

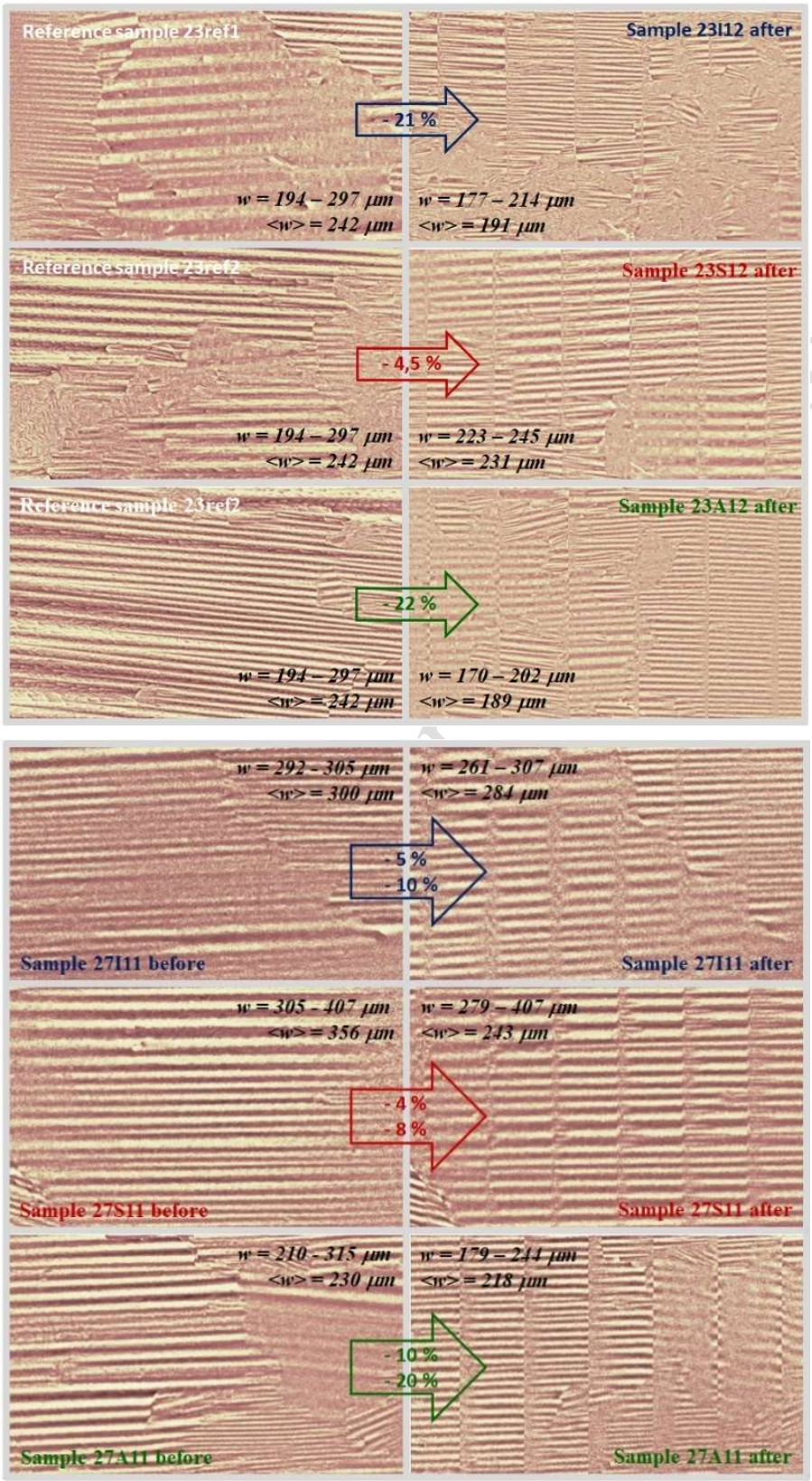

Fig. 4. Magnetic domains imaging for LPL (I), SPL (S) and USPL (A) on grade 23MXX after a double sided process (top) and on grade RXXX27 after a single sided process (bottom) with the MOIF technique.

$$V^2(z) = \Lambda_0^{-2}\frac{\cosh\left(\sqrt{\kappa(1+j\tau\omega)}z\right)}{\cosh\left(\sqrt{\kappa(1+j\tau\omega)}\frac{\zeta}{2}\right)}(z\text{: coordinate // Normal Direction (ND)}) \quad (2a)$$

$$J = \frac{1}{\zeta}\left(\int_{-\frac{\zeta}{2}}^{+\frac{\zeta}{2}} V^2(z)dz\right)\frac{\Lambda_0^2}{[1+j\sigma\Lambda_0^2\mu\omega]}\mu H_0 = \frac{\tanh\left(\sqrt{\kappa(1+j\tau\omega)}\frac{\zeta}{2}\right)}{\sqrt{\kappa(1+j\tau\omega)}\frac{\zeta}{2}(1+j\sigma\Lambda_0^2\mu\omega)}\mu H_0 \quad (2b)$$

$$\mu_{app} = \frac{B}{H_0} \approx \frac{J}{H_0} = \frac{\tanh\left(\sqrt{\kappa(1+j\tau\omega)}\frac{\zeta}{2}\right)}{\sqrt{\kappa(1+j\tau\omega)}\frac{\zeta}{2}(1+j\sigma\Lambda_0^2\mu\omega)}\mu \quad (2c)$$

$$P_s \approx Real_{\omega\to 0}\left(-j\omega\frac{\pi\cdot H_0\cdot J^*}{\gamma}\right) = \nu_c\frac{\tanh\left(\sqrt{\kappa}\frac{\zeta}{2}\right)}{\sqrt{\kappa}\frac{\zeta}{2}}\cdot\frac{B^2\omega}{2\gamma} \quad (2d)$$

$$P_d \approx Real\left(\omega\frac{\pi\sigma\Lambda_0^2\omega\cdot J_0\cdot J^*}{\gamma}\right) = \sigma\Lambda_0^2.Real\left(\frac{(1+j\sigma\Lambda_0^2\mu\omega)\sqrt{\kappa(1+j\tau\omega)}\frac{\zeta}{2}}{\tanh\left(\sqrt{\kappa(1+j\tau\omega)}\frac{\zeta}{2}\right)}\right)\cdot\frac{B^2\omega^2}{2\gamma} \quad (2e)$$

4. Magnetic structure

Surface magnetic domains shape, length and especially width w are observed with the MOIF technique (Fig. 4). The observation of magnetic domains allows to estimate the statistical average of domains' width <w> defined in equation (3). In fact, MOIF images of domains can be analyzed with the FFT technique in 2D (see Fig. 5 and Fig. 6). The geometrical parameter <w> is thus obtained thanks to the median value $\bar{k}$ of spatial frequency k in the probability density spectra of the domains' size in the transverse direction (TD).

$$\langle w\rangle = \frac{1}{n.S} = \frac{1}{2\bar{k}} \quad (3)$$

Fig. 5 and Fig. 6 show that all the laser processes are able to refine the magnetic domains with low spatial frequencies k by increasing the population of domains with higher spatial frequencies.

Table 3 : Domains' width refinement

	LPL (%)	SPL (%)	USPL 1 A12 (%)
0,23	-21 %	-5 %	-22 %
0,27	-8 %	-6 %	-15 %

The increase of probability density with the highest k, leading to the most significant refinement effect, is obtained for the USPL process on two investigated conventional grades of $Si_{w3.3\%}Fe_{w96.7\%}$ GOES with thicknesses 0.23 and 0.27 mm (23I12(-21%), 23S12(-5%), **23A12(-22%)** and 27I11(-8%), 27S11(-6%), **27A12(-15%)**) (Table 3). The connection between the identified property Λ, the width w and the mobility η is obtained with equation (4a). The change in mobility $d\eta$ can be expressed as a function of both variations dw and $d\Lambda$ (4b).

$$\Lambda \propto \sqrt{\frac{w}{2\sigma J_s\eta}} \quad (4a)$$

$$d\eta \propto \left(\frac{dw}{2\sigma J_s\Lambda^2} - \frac{wd\Lambda}{\sigma J_s\Lambda^3}\right) \quad (4b)$$

J_s is the saturation magnetic polarization.

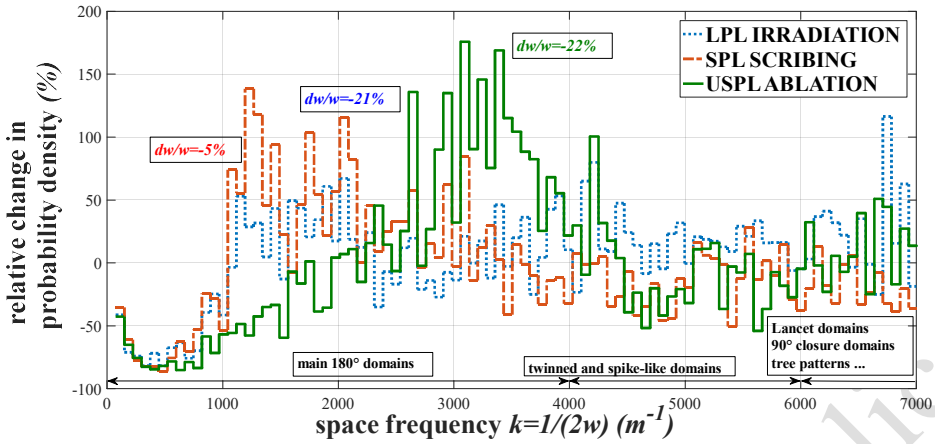

Fig. 5 : Domains refinement distribution of grade 23MXX (average of 8 images per process v.s. reference samples).

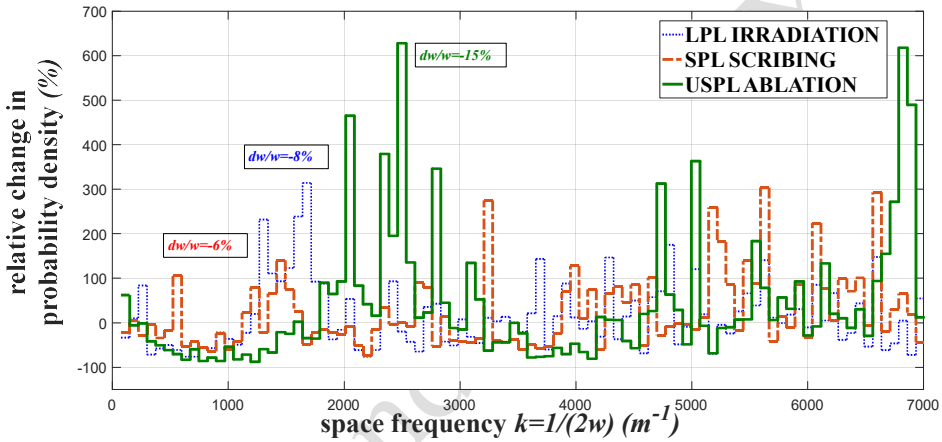

Fig. 6 : Domains refinement distribution of grade RXXX27 (comparisons on the same samples before and after).

5. Identifications and Cross Comparisons

The different microscopic physical origins of loss reduction depending on the type of laser process used can be identified and clarified by looking at the results of Fig. 7 and Fig. 8, on top for grade 23MXX and at the bottom for grade RXXX27.

Any surface domains refinement will act on Λ and Λ_0, laser induced stress on μ and κ, induced pinning centers on $\underline{\nu_c}$ and ν_c and any walls nucleation, multiplication and mobility effect will be visible on η and τ. It seems to be not only a question of domains refinement!

A first result obtained whatever the model is that the use of LPL and SPL at both sides of the thicker material failed to reduce even more the losses like it is the case for the USPL. On low thicknesses (Fig. 2), a second side or a second pass is beneficial mainly for P_d but detrimental for P_s. For higher thicknesses (Fig. 3), both USPL A12 and A21 are able to reduce both P_s and P_d. The heat required to sufficiently stress the laser spots inside the entire thickness must be increased in the thick grade and this might enlarge the HAZ too much when applying the LPL or SPL process at both sides which is detrimental for the magnetic performances. One solution proposed is to create grooves either at both sides or with two passes without any heat generated thanks to the USPL ablation process. For the average μ-$\underline{\nu_c}$-Λ model first in Fig. 7, it seems clear that there still cannot be any distinction between the different pulse durations at high induction levels (see **Erreur ! Source du renvoi introuvable.** and Fig. 3 B>1.7T). At 1.7 T and above, the whole properties and therefore the loss reduction factors tends towards more or less the same values (Fig. 2, Fig. 3 and Table 4). An exception occurs for the impact of USPL ablation A12 and A21 processes on the quasi static internal permeability μ which can be more impacted than the others: at high induction level, the permeability μ is damaged, at low induction level B, the permeability μ is enhanced. The behavior is exacerbated for the USPL. Nevertheless, a clear distinction between the different pulse durations is identified for low and intermediate induction levels, below 1.5 T. The LPL irradiation process is able to reduce more the coercive reluctivity $\underline{\nu_c}$ than the SPL scribing process that generates too much heat during the engraving process. The difference is more significant for the low thickness. USPL ablation A21 is the only one able to reduce even more $\underline{\nu_c}$ for both thicknesses. Thanks to deep enough grooves without HAZ at both sides, the process A12 is a compromise between irradiation and scribing for the low thickness but works as well as A21 for the

thick sheet. On the contrary, the SPL scribing process is able to improve more the dynamical properties Λ (reduction) and η (increase) than the LPL irradiation process, probably due to the absence of magnetic poles in a groove and the presence of a residual stress still enforced by the coating. The improvements and differences are more significant for the low thickness. Again, USPL ablation A21 is the only one able to improve even more Λ and η for both thicknesses. Thanks to clean grooves at both sides, maximizing the magnetic poles induced refinement and the walls dynamics, the process A12 is a compromise between irradiation and scribing for the low thickness but works as well as and even better than A21 for the thick sheet.

For the average TMPT model then in Fig. 8, discriminating the different processes is possible for all the model parameters. In this model, the impact on the permeability is explained by the laser stress induced anisotropic exchange property κ which is decreased at low B and increased at high B, this phenomenon is exacerbated for low thicknesses and the USPL ablation processes. The deeper grooves generated by the USPL ablation processes would act at high B like walls pinning spots that significantly increase the coercive reluctivity ν_c for both thicknesses. At low B, and for the thick sheet, ablation grooves can become either walls' activation or multiplication centers, similar to inclusions, which can reduce the coercive reluctivity ν_c. more significantly than the other techniques. The USPL ablation process seems also able to reduce the dynamical properties Λ_0 and τ more than the LPL and the SPL processes, probably thanks to the presence of magnetic poles in a groove and the absence of any residual stress. The improvements and differences are larger for the low thickness. USPL ablation A21 is still the only one able to improve even more Λ_0 for both thicknesses. Thanks to deep grooves at one side, A21 is maximizing the magnetic poles induced refinement mainly at the sheet surface, which contributes to the significant decrease of property Λ_0. Thanks to clean grooves at both sides, A12 is optimizing the number of nucleation and multiplication centers at each side of the sheet; which helps the walls dynamics inside the volume and contributes to the most significant decrease of damping delay τ.

6. Conclusion and Perspectives

Cross comparisons between the model, experiments and the observations allow to identify some discriminating physical principles behind the changes in magnetic structure due to different pulsed laser impacts. The method separates the quasi-static ($\underline{\nu_c}$ or ν_c), self-organizing (μ or κ), topological (domains size Λ or Λ_0) and dynamical (η or τ) origins of the behavior and discriminates between different laser processes. This work also provides data for the field diffusion-like [12] and the boundary TMPT formulation [13] usable when integrating the electrical sheets in a magnetic core. The process optimization finally leads to the best performances for each laser configuration and both GOES grades with thicknesses 0.23 and 0.27 mm @1.7T50Hz given in Table 4.

Table 4 : Loss reduction factors at 1.7 T and 50 Hz

1,7T 50HZ	LPL (%)	SPL (%)	USPL 1 A12 (%)	USPL 2 A21 (%)
0,23	**-17,5 (I12)**	**-16,4 (S12)**	**-19,3**	**-13,4**
0,27	**-15,3 (I11)**	**-11 (S11)**	**-15,3**	**-15,4**

However, it must be mentioned that no laser impact on the shape of hysteresis loops (including the coercive field) can be accurately determined as long as neither DC magnetic measurements or extrapolations nor non-linear hysteresis models are proposed within the TMPT. The complete faithful description, including the microscopic point of view, requires to analyse further the shape and dynamics of walls and domains at the vicinity of and in between the laser spots at the microscopic and nanoscopic scales [14]. Only properties in the Rolling Direction (RD) have been investigated. As a first perspective, the same cross comparisons have to be implemented in order to discriminate the different pulsed laser processes that are able to optimize the magnetic performances in the other directions, either in the Transverse Direction (TD) or in a flux direction that makes an arbitrary angle with the Rolling Direction (RD) [15].

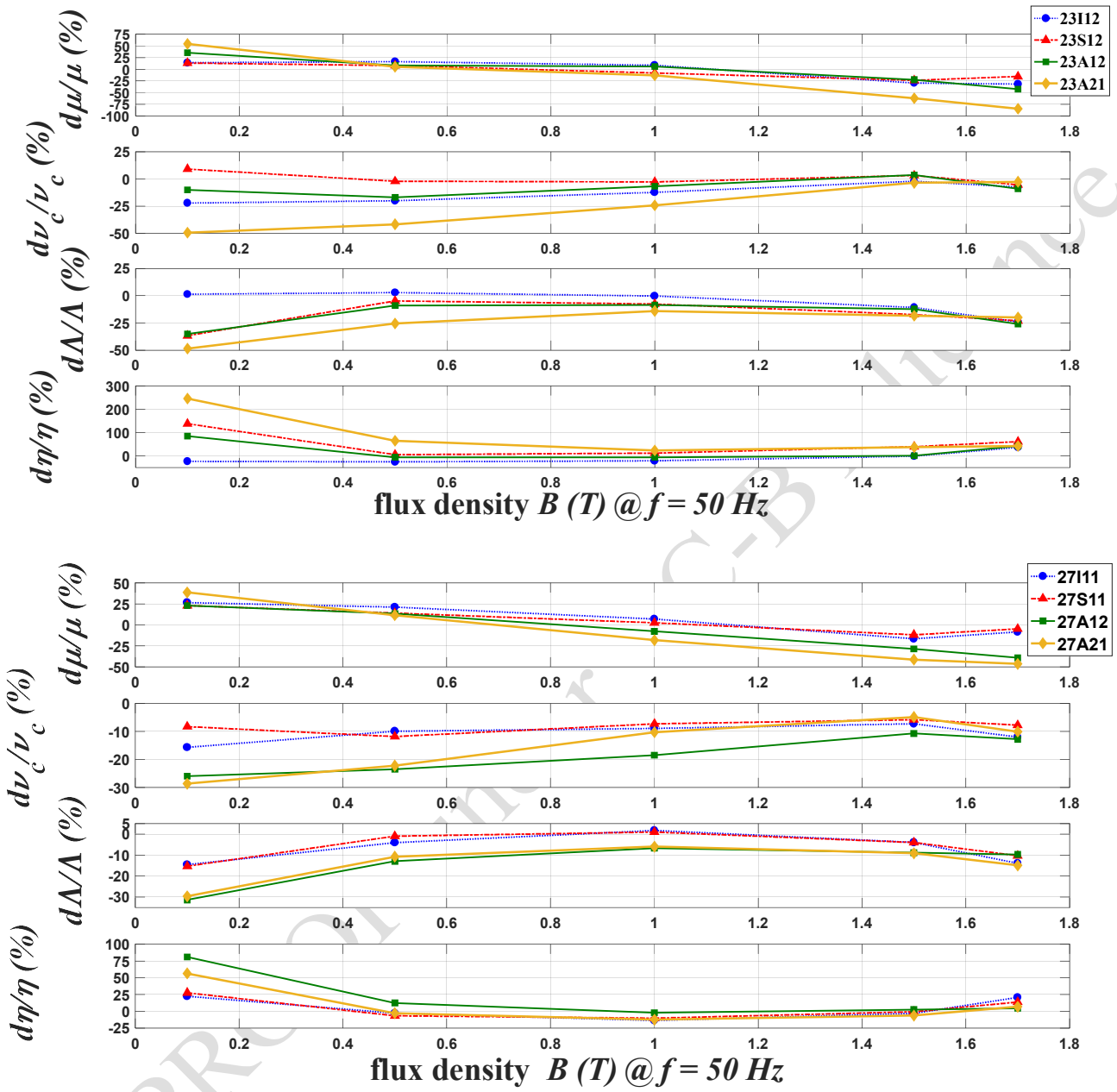

Fig. 7 : Impact of lasers on μ-$\underline{\nu_c}$-Λ magnetic properties of grade 23MXX (left) and grade RXXX27 (right).

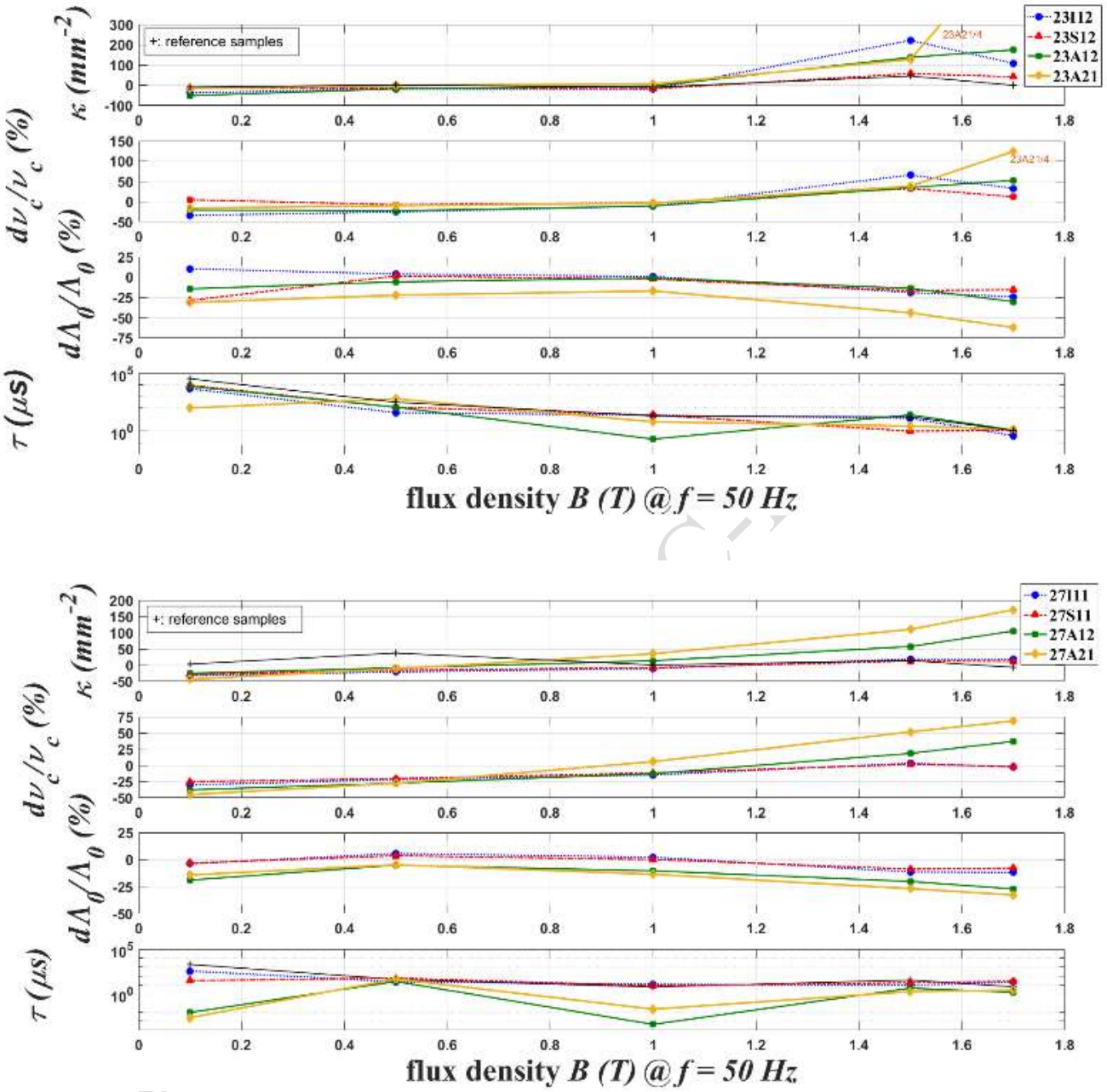

Fig. 8 : Impact of lasers on TMPT magnetic properties of grade 23MXX (left) and grade RXXX27 (right).

References

[1] P. Beckley and D. Snell, "Low-Cost, High-Speed Domain Refinement without Damage to Insulative Coatings", Journal of Materials Engineering and Performance, vol. 3, pp. 209-213, Apr. 1994. https://doi.org/10.1007/BF02645844
[2] K. Sato, M. Kurosawa, B. Fukuda, T. Kan, "Investigation on the domain refining effect in grain-oriented silicon steel", JMMM, vol. 112, no. 1-3, pp. 183-185, july 1992.
[3] P. Beckley, D. Snell, C. Lockhart, "Domain control by spark ablation", J. Appl. Phys. 57 (8) (april 1985) 4212–4213.
[4] S. V. Ponnaluri, R. Cherukuri, P.A. Molian, "Core loss reduction in grain-oriented silicon steels by excimer laser scribing: Part I: experimental work",J. Mat. Proc. T., vol. 112, no. 2–3, pp. 199–204, 2001.
[5] Y. Huang et al., "Parameter optimization of Nd:Yag laser scribing process on core loss of grain-oriented magnetic silicon steels", Int. J. Adv. Manuf. Technol., vol. 70, pp. 1-9, Jan. 2014.
[6] I. Petryshynets et al., "Magnetic losses reduction in grain oriented silicon steel by pulse and continuous fiber laser processing," AIP Advances, vol. 8, no. 047604, 2018.
[7] M. Nesser et al., "Influence of a laser irradiation and laser scribing on magnetic properties of GO silicon steels sheets using a nanosecond fiber laser", EJEE, vol. 23, n°6, Dec. 2021, pp. 439-444.
[8] J. Dupuy et al., "Comparison between laser thermal effects and ablation effects with ultrashort pulsed laser on GO SiFe electrical steel", SPIE LASE conf., USA (2019), Proc. vol. 10911, 2505326.
[9] M. Nesser et al., "Correlation between laser energetic parameters and magnetic properties of GO laminations under surface treatments with long, short or ultra-short pulsed lasers", JMMM, vol. 504, 15 June 2020, 166696.
[10] M. Nesser et al., "Impact of Ultra-Short Pulsed Laser (USPL) Ablation Process on Separated Loss Coefficients of Grain Oriented Electrical Steels", IEEE Transactions on Magnetics, vol. 58 (8), 2022, 2001105, doi: 10.1109/TMAG.2022.3152899.
[11] G. Bertotti, "General properties of power losses in soft ferromagnetic materials", IEEE Trans. Magn., vol. 24, no. 1, 1988, pp. 621–630.
[12] O. Maloberti et al., "Sheet thickness dependence of magnetization properties based on domains and walls within the non-linear diffusion-like equation for Grain Oriented Electrical Steels", JMMM, vol. 557, sept. 2022, 169349.
[13] O. Maloberti et al., "The Tensor Magnetic Phase Theory for mesoscopic volume structures of soft magnetic materials – Quasi-static and dynamic vector polarization, apparent permeability and losses – Experimental identifications of GO steel at low induction levels", JMMM, vol. 502, May 2020, 166403.
[14] M. Nesser et al., "Microscopic Magnetic Domain Structure of GOES at the Vicinity of and On the Laser Lines Post-Laser Treatment with Different Pulse Durations", 25th SMM Conf., Grenoble 2022.
[15] P. Dupont et al., "Experimental impact of pulsed laser irradiation, scribing and ablation on 2-D scalar and vector magnetic losses and general properties of Grain-Oriented Electrical Steels", INTERMAG conf. paper, 2021, pp. 1-5.

Acknowledgements

We thank APERAM Brazil and SEPSA for having given samples of GOES with thickness 0,27-0,28 mm and 0,23 mm. The project ESSIAL received funding from the European Research Council under the H2020-IND-CE-2016-17/H2020-FOF-2017 Program (Grant No. 766437).